

Orbital fluctuations in the RVO_3 perovskites

Andrzej M. Oleś and Peter Horsch

Abstract The properties of Mott insulators with orbital degrees of freedom are described by spin-orbital superexchange models, which provide a theoretical framework for understanding their magnetic and optical properties. We introduce such a model derived for $(xy)^1(yz/zx)^1$ configuration of V^{3+} ions in the RVO_3 perovskites, $R=Lu, Yb, \dots, La$, and demonstrate that $\{yz, zx\}$ orbital fluctuations along the c axis are responsible for the huge magnetic and optical anisotropies observed in the almost perfectly cubic compound $LaVO_3$. We argue that the $GdFeO_3$ distortion and the large difference in entropy of C -AF and G -AF phases is responsible for the second magnetic transition observed at T_{N2} in YVO_3 . Next we address the variation of orbital and magnetic transition temperature, T_{OO} and T_{N1} , in the RVO_3 perovskites, after extending the spin-orbital model by the crystal-field and the orbital interactions which arise from the $GdFeO_3$ and Jahn-Teller distortions of the VO_6 octahedra. We further find that the orthorhombic distortion which increases from $LaVO_3$ to $LuVO_3$ plays a crucial role by controlling the orbital fluctuations, and via the modified orbital correlations influences the onset of both magnetic and orbital order.

1 Orbital degrees of freedom in strongly correlated systems

Orbital degrees of freedom play a key role for many intriguing phenomena in strongly correlated transition metal oxides, such as the colossal magnetoresistance in the manganites or the effective reduction of dimensionality in $KCuF_3$ [1]. Before

Andrzej M. Oleś

M. Smoluchowski Institute of Physics, Jagellonian University, Reymonta 4, 30059 Kraków, Poland
Max-Planck-Institut für Festkörperforschung, Heisenbergstrasse 1, 70569 Stuttgart, Germany
e-mail: A.M.Oles@fkf.mpg.de

Peter Horsch

Max-Planck-Institut für Festkörperforschung, Heisenbergstrasse 1, 70569 Stuttgart, Germany
e-mail: P.Horsch@fkf.mpg.de

addressing complex phenomena in doped Mott insulators, it is necessary to describe first the undoped materials, such as LaMnO_3 or LaVO_3 . These two systems are canonical examples of correlated insulators with coexisting magnetic and orbital order [1]. In both cases large local Coulomb interaction U suppresses charge fluctuations, leading to low-energy effective Hamiltonians with superexchange interactions which stabilize antiferromagnetic (AF) spin order at low temperature [2, 3]. However, the AF order is different in both cases: ferromagnetic (FM) planes are coupled by AF interactions in the A -type AF phase of LaMnO_3 , while FM chains along the c cubic axis are coupled by AF interactions in the ab planes in the C -type AF (C -AF) phase of LaVO_3 . The superexchange Hamiltonians which describe both systems are just examples for the spin-orbital physics [4], where orbital (pseudospin) operators contribute explicitly to the structure of the superexchange interactions — their actual form depends on the number of $3d$ electrons (holes) at transition metal ions which determines the value of spin S , and on the type of active orbital degrees of freedom, e_g or t_{2g} . In simple terms, the magnetic structure is determined by the pattern of occupied and empty orbitals, and the associated rules are known as Goodenough-Kanamori rules (GKR). The central focus of this overview are t_{2g} orbital degenerate systems, where quantum fluctuations of orbitals play a central role for the electronic properties [3, 5, 6] and modify the predictions of the GKR.

In the last two decades several new concepts were developed in the field of orbital physics [1]. The best known spin-orbital superexchange Hamiltonian is the Kugel-Khomskii model [7], which describes the e_g orbital $\{x^2 - y^2, 3z^2 - r^2\}$ degrees of freedom coupled to $S = 1/2$ spins at Cu^{2+} (d^9) ions in KCuF_3 . The spins interact by either FM and AF exchange interactions, depending on the type of occupied and empty orbitals on two neighboring ions. It has been found that enhanced quantum fluctuations due to orbital degrees of freedom, which contribute to joint spin-orbital dynamics, may destabilize long-range magnetic order near the quantum critical point of the Kugel-Khomskii model [8]. The orbital part of the superexchange is thereby intrinsically frustrated even on geometrically non-frustrated lattices, as in the perovskite lattice [8, 9], which is a second important concept in the field of orbital physics. Finally, although spin and orbital operators commute, there are situations where joint spin-orbital dynamics plays a crucial role, and spin and orbital operators cannot be separated from each other. This situation is called spin-orbital entanglement [10], and its best example are the entangled $\text{SU}(4)$ singlets in the one-dimensional (1D) $\text{SU}(4)$ model [11]. There is no doubt that these recent developments in the orbital physics provide many challenges both for the experimental studies and for the theoretical understanding of the experimental consequences of the spin-orbital superexchange.

Let us consider first the orbital part of the superexchange. Its intrinsic frustration results from the directional nature of orbital pseudospin interactions [8, 9] — they imply that the pair of orbitals which would minimize the energy depends on the direction of a bond $\langle ij \rangle$ in a cubic (perovskite) lattice. In case of e_g orbitals the superexchange interactions are Ising-like as only one orbital flavor allows for electron hopping t and the electron exchange process does not occur. They favor a pair of orthogonal orbitals on both sites of the considered bond [12], for instance

$|z\rangle \sim (3z^2 - r^2)/\sqrt{6}$ and $|x\rangle \sim x^2 - y^2$ orbital for a bond along the c axis. When the two above orbital states are represented as components of $\tau = 1/2$ pseudospin, this configuration gives the energy of $-\frac{1}{4}J$, where J is the superexchange constant. Unlike in the 1D model [13], such an optimal orbital configuration cannot be realized simultaneously on all the bonds in a two-dimensional (2D) or three-dimensional (3D) system. Thus, in contrast to spin systems, the tendency towards orbital disordered state (orbital liquid) is *enhanced* with increasing system dimension [14, 15].

The essence of orbital frustration is captured by the 2D compass model, originally developed as a model for Mott insulators [7]. Intersite interactions in the compass model are described by products $\tau_i^\alpha \tau_j^\alpha$ of single pseudospin components,

$$\tau_i^x = \frac{1}{2}\sigma_i^x, \quad \tau_i^y = \frac{1}{2}\sigma_i^y, \quad \tau_i^z = \frac{1}{2}\sigma_i^z. \quad (1)$$

for a bond $\langle ij \rangle \parallel \gamma$, where $\alpha = x, y, z$, rather than by a pseudospin scalar product $\tau_i \cdot \tau_j$. For instance, in the 2D case of a single ab plane, the compass model [16],

$$H_{2D} = J_x \sum_{\langle ij \rangle \parallel a} \tau_i^x \tau_j^x + J_z \sum_{\langle ij \rangle \parallel b} \tau_i^z \tau_j^z, \quad (2)$$

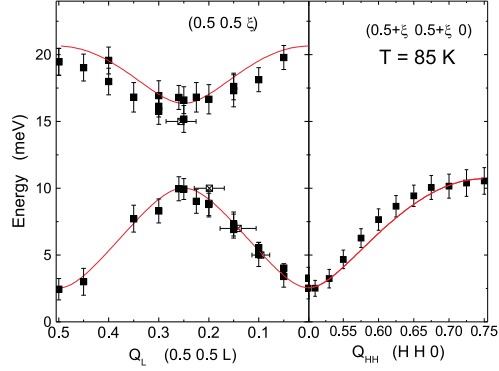
describes the competition between $\tau_i^x \tau_j^x$ and $\tau_i^z \tau_j^z$ interactions for the bonds along a and b axis, respectively. This competition of pseudospin interactions along different directions results in intersite correlations similar to those in the anisotropic XY model, and generates a quantum critical point at $J_x = J_z$, with high degeneracy of the ground state [17]. So, despite certain similarities of the compass model to ordinary models used in quantum magnetism, an ordered phase with finite magnetization is absent. It is interesting to note that a similar quantum phase transition exists also in the 1D chain compass model [18] ($N' = N/2$ is the number of unit cells):

$$H_{1D} = \sum_{i=1}^{N'} \{J_x \tau_{2i-1}^x \tau_{2i}^x + J_z \tau_{2i}^z \tau_{2i+1}^z\}. \quad (3)$$

Recently this 1D compass model was solved exactly in the whole range of $\{J_x, J_z\}$ parameters [18] by mapping to the exactly solvable (quantum) Ising model in transverse field. It provides a beautiful example of a first order quantum phase transition between two phases with large $\langle \tau_{2i-1}^x \tau_{2i}^x \rangle$ or $\langle \tau_{2i}^z \tau_{2i+1}^z \rangle$ correlations, and discontinuous changes of intersite correlation functions.

In realistic spin-orbital superexchange models transitions between different ordered or disordered orbital states are accompanied by magnetic transitions. This field is very rich, and several problems remain unsolved as simple mean-field (MF) approaches do not suffice in general, even for the systems with perovskite lattices [4]. In this chapter we shall address the physical properties of the RVO_3 perovskites ($R=\text{Lu, Yb, } \dots, \text{La}$), where not only the above intrinsic frustration of the orbital superexchange, but also the structure of the spin-orbital superexchange arising from multiplet splittings due to Hund's exchange plays a role and determines the observed physical properties at finite temperature. Moreover, we shall see that the cou-

Fig. 1 Magnon dispersion relation obtained by neutron scattering for the C-AF phase of YVO_3 at $T = 85$ K. The lines are interpolation between the experimental points (squares with error bars) along two high symmetry directions in the Brillouin zone. Image courtesy of Clemens Ulrich.



pling of the orbitals to the lattice, i.e., via Jahn-Teller (JT) coupling, GdFeO_3 -like and orthorhombic distortion, are important control parameters. First we analyze the structure of the spin-orbital superexchange in section 2 and show its consequences for the magnetic and optical properties of strongly correlated transition metal compounds. Here we also address the entanglement of spin and orbital variables which is ignored in the MF decoupling, and we point out that it fails in certain situations.

The coupling between the orbital and spin variables is capable of generating qualitatively new phenomena which do not occur in the absence of orbital interactions, such as anisotropic magnetic interactions, and novel quantum phenomena at finite temperature, discussed on the example of LaVO_3 in section 3. One of such novel and puzzling phenomena is the magnetic phase transition between two different types of AF order observed in YVO_3 — this compound has G -type AF order (staggered in all three directions, called below G -AF phase) at low temperature $T < T_{N2}$, while the magnetic order changes in the first order magnetic transition at $T_{N2} = 77$ K to C -AF phase which remains stable up to $T_{N1} \simeq 116$ K. The latter C -AF phase has rather exotic magnetic properties, and the magnon spectra show dimerization of the FM interactions along the c axis [19], see figure 1. In fact, the G -AF phase occurs in systems with large GdFeO_3 -like distortion [20]. In Ref. [3] an orbital interaction favoring C -type alternating orbital (C -AO) order was invoked to explain the G -AF phase. We also address this problem in section 3 and present arguments that at higher $T > T_{N2}$ C -AF phase reappears is due to its higher entropy [3].

In section 4 we address the experimental phase diagram of the RVO_3 perovskites. It is quite different from the (also puzzling) phase diagram of the RMnO_3 perovskites, where the orbital order (OO) appears first at T_{OO} upon lowering the temperature, and spin order follows [21] at the Néel temperature, $T_{N1} \ll T_{OO}$. In contrast, in the RVO_3 perovskites the two transitions appear at similar temperature [22]. For instance, in LaVO_3 they occur even almost simultaneously i.e., $T_{N1} \simeq T_{OO}$. However, they become separated from each other in the RVO_3 systems with smaller ionic radii of R ions — whereas T_{N1} gets reduced for decreasing r_R , T_{OO} exhibits a *nonmonotonic* dependence on r_R [20]. A short summary is presented in section 5. We also point out a few unsolved problems of current interest in the field of orbital physics.

2 Spin-orbital superexchange and entanglement

Spin-orbital models derived for real systems are rather complex and the orbital part of the superexchange is typically much more complicated than the compass model (2) of section 1 [4]. The main feature of these superexchange models is that not only the orbital interactions are directional and frustrated, but also spin correlations may influence orbital interactions and *vice versa*. This is best seen in the Kugel-Khomskii (d^9) model [7], where the G -AF and A -AF order compete with each other, and the long-range order is destabilized by quantum fluctuations in the vicinity of the quantum critical point $(J_H, E_z) = (0, 0)$ [23]. Here J_H is the local exchange (see below), and E_z is the splitting of two e_g orbitals. Although this model is a possible realization of disordered spin-orbital liquid, its phase diagram remains unexplored beyond the MF approach and simple valence-bond wave functions of Ref. [8] — it remains one of the challenges in this field.

In this chapter we consider the superexchange derived for an (idealized) perovskite structure of RVO_3 , with V^{3+} ions occupying the cubic lattice. The kinetic energy is given by:

$$H_t = -t \sum_{\langle ij \rangle \| \gamma} \sum_{\alpha(\gamma), \sigma} \left(d_{i\alpha\sigma}^\dagger d_{j\alpha\sigma} + d_{j\alpha\sigma}^\dagger d_{i\alpha\sigma} \right), \quad (4)$$

where $d_{i\alpha\sigma}^\dagger$ is electron creation operator for an electron with spin $\sigma = \uparrow, \downarrow$ in orbital α at site i . The summation runs over the bonds $\langle ij \rangle \| \gamma$ along three cubic axes, $\gamma = a, b, c$, with the hopping elements t between active t_{2g} orbitals. They originate from two subsequent hopping processes via the intermediate $2p_\pi$ oxygen orbital along each V–O–V bond. Its value can in principle be derived from the charge-transfer model [24], and one expects $t = t_{pd}^2/\Delta \sim 0.2$ eV [3]. Only two out of three t_{2g} orbitals, labelled by $\alpha(\gamma)$, are active along each bond $\langle ij \rangle$ and contribute to the kinetic energy (4), while the third orbital lies in the plane perpendicular to the γ axis and the hopping via the intermediate oxygen $2p_\pi$ oxygen is forbidden by symmetry. This motivates a convenient notation used below,

$$|a\rangle \equiv |yz\rangle, \quad |b\rangle \equiv |xz\rangle, \quad |c\rangle \equiv |xy\rangle, \quad (5)$$

where the orbital inactive along a cubic direction γ is labelled by its index as $|\gamma\rangle$.

The superexchange model for the RVO_3 perovskites arises from virtual charge excitations between V^{3+} ions in the high-spin $S = 1$ state. The number of d electrons is 2 at each V^{3+} ion (d^2 configuration), and the superexchange is derived from all possible virtual $d_i^2 d_j^2 \rightleftharpoons d_i^3 d_j^1$ excitation processes (for more details see Ref. [25]). It is parametrized by the superexchange constant J and Hund's parameter η ,

$$J = \frac{4t^2}{U}, \quad \eta = \frac{J_H}{U}, \quad (6)$$

where U is the intraorbital Coulomb interaction and J_H is Hund's exchange between t_{2g} electrons. Here we use the usual convention and write the local Coulomb inter-

actions between $3d$ electrons at V^{3+} ions by limiting ourselves to intraorbital and two-orbital interaction elements [4]:

$$H_{\text{int}} = U \sum_{i\alpha} n_{i\alpha\uparrow} n_{i\alpha\downarrow} + \left(U - \frac{5}{2} J_H \right) \sum_{i,\alpha<\beta} n_{i\alpha} n_{i\beta} - 2J_H \sum_{i,\alpha<\beta} \mathbf{S}_{i\alpha} \cdot \mathbf{S}_{i\beta} + J_H \sum_{i,\alpha<\beta} \left(d_{i\alpha\uparrow}^\dagger d_{i\alpha\downarrow}^\dagger d_{i\beta\downarrow} d_{i\beta\uparrow} + d_{i\beta\uparrow}^\dagger d_{i\beta\downarrow}^\dagger d_{i\alpha\downarrow} d_{i\alpha\uparrow} \right). \quad (7)$$

When only one type of orbitals is partly occupied (as in the present case of the RVO_3 perovskites or in $KCuF_3$), the two parameters $\{U, J_H\}$ are sufficient to describe these interactions in Eq. (7): (i) the intraorbital Coulomb element U and (ii) the interorbital (Hund's) exchange element J_H , where $\{A, B, C\}$ are the Racah parameters [26]. In such cases the above expression is exact; in other cases when both e_g and t_{2g} electrons contribute to charge excitations (as for instance in the $RMnO_3$ perovskites), Eq. (7) is only an approximation — the anisotropy on the interorbital interaction elements has to be then included to reproduce accurately the multiplet spectra of the transition metal ions [26]. The intraorbital interaction is $U = A + 4B + 3C$, while J_H depends on orbital type — for t_{2g} electrons one finds [4, 26] $J_H = 3B + C$.

The perturbative treatment of intersite charge excitations $d_i^2 d_j^2 \Rightarrow d_i^3 d_j^1$ in the regime of $t \ll U$ leads for the RVO_3 perovskites (and in each similar case [4]) to the spin-orbital superexchange model:

$$\mathcal{H}_J = \sum_{\langle ij \rangle \parallel \gamma} H^{(\gamma)}(ij) = J \sum_{\langle ij \rangle \parallel \gamma} \left\{ (\mathbf{S}_i \cdot \mathbf{S}_j + S^2) \hat{J}_{ij}^{(\gamma)} + \hat{K}_{ij}^{(\gamma)} \right\}. \quad (8)$$

The spin interactions $\propto \mathbf{S}_i \cdot \mathbf{S}_j$ obey the $SU(2)$ symmetry. In contrast, the orbital interaction operators $\hat{J}_{ij}^{(\gamma)}$ and $\hat{K}_{ij}^{(\gamma)}$ involve directional (here t_{2g}) orbitals on each individual bond $\langle ij \rangle \parallel \gamma$, so they have a lower (cubic) symmetry. The above form of the spin-orbital interactions is general and the spin value S depend on the electronic configuration d^n of the involved transition metal ions (here $n = 2$ and $S = 1$). For convenience, we introduced also a constant S^2 in the spin part, so for the classical Néel order the first term $\propto \hat{J}_{ij}^{(\gamma)}$ vanishes.

In the RVO_3 perovskites one finds the orbital operators [25]:

$$\hat{J}_{ij}^{(\gamma)} = \frac{1}{2} \left\{ (1 + 2\eta r_1) \left(\boldsymbol{\tau}_i \cdot \boldsymbol{\tau}_j + \frac{1}{4} n_i n_j \right) - \eta r_3 \left(\boldsymbol{\tau}_i \times \boldsymbol{\tau}_j + \frac{1}{4} n_i n_j \right) - \frac{1}{2} \eta r_1 (n_i + n_j) \right\}^{(\gamma)}, \quad (9)$$

$$\hat{K}_{ij}^{(\gamma)} = \left\{ \eta r_1 \left(\boldsymbol{\tau}_i \cdot \boldsymbol{\tau}_j + \frac{1}{4} n_i n_j \right) + \eta r_3 \left(\boldsymbol{\tau}_i \times \boldsymbol{\tau}_j + \frac{1}{4} n_i n_j \right) - \frac{1}{4} (1 + \eta r_1) (n_i + n_j) \right\}^{(\gamma)}, \quad (10)$$

where the scalar product $(\boldsymbol{\tau}_i \cdot \boldsymbol{\tau}_j)^{(\gamma)}$ and the cross-product,

$$(\boldsymbol{\tau}_i \times \boldsymbol{\tau}_j)^{(\gamma)} = \frac{1}{2} \left(\boldsymbol{\tau}_i^+ \boldsymbol{\tau}_j^+ + \boldsymbol{\tau}_i^- \boldsymbol{\tau}_j^- \right) + \boldsymbol{\tau}_i^z \boldsymbol{\tau}_j^z, \quad (11)$$

involve orbital (pseudospin) operators corresponding to two active t_{2g} orbitals along the γ axis, with $\boldsymbol{\tau}_i = \{ \boldsymbol{\tau}_i^+, \boldsymbol{\tau}_i^-, \boldsymbol{\tau}_i^z \}$, and

$$\boldsymbol{\tau}_i^z = \frac{1}{2} (n_{i,yz} - n_{i,zx}). \quad (12)$$

They follow from the structure of local Coulomb interaction (7). The latter term (11) leads to the nonconservation of total pseudospin quantum number. Density operators $n_i^{(\gamma)}$ in Eqs. (9) and (10) stand for the number of d electrons in active orbitals for the considered bond $\langle ij \rangle$, e.g. $n_i^{(c)} = n_{ia} + n_{ib}$. The coefficients,

$$r_1 = \frac{1}{1 - 3\eta}, \quad r_3 = \frac{1}{1 + 2\eta}, \quad (13)$$

follow from the energies of $d_i^2 d_j^2 \Rightarrow d_i^3 d_j^1$ excitations in the units of U : (i) r_1 represents the high-spin 4A_2 excitation of energy $(U - 3J_H)$, while the low-spin excitations are given by (ii) $r_2 = 1$ originating from the low-spin 2T_1 and 2E excitations of energy U , and (iii) r_3 represents the low-spin 2T_2 states of energy $(U + 2J_H)$.

Magnetic order observed in Mott insulators is usually understood in terms of the GKR which are based on the MF picture and ignore entangled quantum states. These rules state that the pattern of occupied orbitals determines the spin structure. For example, for 180° bonds (e.g. Mn–O–Mn bonds in LaMnO_3) there are two key rules: (i) if two partially occupied $3d$ orbitals point towards each other, the interaction is AF, however, (ii) if an occupied orbital on one site has a large overlap with an empty orbital on the other site of a bond $\langle ij \rangle$, the interaction is weak and FM due to finite Hund's exchange. This means that spin order and orbital order are complementary — ferro-like (uniform) orbital (FO) order supports AF spin order, while AO order supports FM spin order. Indeed, these celebrated rules are well followed in LaMnO_3 [27] and in KCuF_3 [28], where strong JT effect stabilizes the orbital order and suppresses the orbital fluctuations. The AO order is here robust in the FM ab planes, while the orbitals obey the FO order along the c axis, supporting the AF coupling and leading to the A-AF phase for both systems. In such cases the GKR directly apply. Therefore, one may disentangle the spin and orbital operators, and it has been shown that this procedure is sufficient to explain both the magnetic [2] and optical [4] properties of LaMnO_3 .

As another prominent example of the Goodenough-Kanamori complementarity we would like to mention the AF phases realized in YVO_3 [19], which are the subject of intense research in recent years. *A priori*, the orbital interactions between V^{3+} ions in d^2 configuration obey the cubic symmetry, if the t_{2g} orbitals are randomly occupied. However, the symmetry breaking at the structural transition where the symmetry is reduced from cubic to orthorhombic, which persists in the magnetic phases, suggests that the electronic configuration is different. Indeed, the GdFeO_3

distortions in the RVO_3 structure break the symmetry in the orbital space, and both the electronic structure calculations [29] and the analysis using the point charge model [30] indicate that the electronic configuration $(xy)^1(yz, zx)^1$ is induced at every site, i.e.,

$$n_{ic} = 1, \quad n_{ia} + n_{ib} = 1. \quad (14)$$

The partly filled $\{a, b\}$ orbitals are both active along the c axis, and may lead either to FO or to AO order. Indeed, depending on this orbital pattern, the magnetic correlations are there either AF or FM, explaining the origin of the two observed types of AF order: (i) the C -AF phase, and (ii) the G -AF phase. However, the situation is more subtle as both orbitals in the orbital doublet $\{|yz\rangle, |xz\rangle\} \equiv \{|a\rangle, |b\rangle\}$ at each site i are active on the bonds along the c axis. This demonstrates an important difference between the e_g (with one electron or one hole in active e_g orbital at each site [13]) and a t_{2g} system, such as RVO_3 perovskite vanadates, where electrons occupying two active t_{2g} orbitals may fluctuate and form an *orbital singlet* [3]. The cubic symmetry is thus broken as both orbital flavors are active only along the c axis, and the bonds in the ab planes and along the c axis are nonequivalent. Consequently, superexchange orbital operators (9) and (10) take different forms along these two distinct directions,

$$\hat{f}_{ij}^{(c)} = \frac{1}{2} \left\{ (1 + 2\eta r_1) \left(\boldsymbol{\tau}_i \cdot \boldsymbol{\tau}_j + \frac{1}{4} \right) - \eta r_3 \left(\boldsymbol{\tau}_i \times \boldsymbol{\tau}_j + \frac{1}{4} \right) - \eta r_1 \right\}, \quad (15)$$

$$\hat{K}_{ij}^{(c)} = \left\{ \eta r_1 \left(\boldsymbol{\tau}_i \cdot \boldsymbol{\tau}_j + \frac{1}{4} \right) + \eta r_3 \left(\boldsymbol{\tau}_i \times \boldsymbol{\tau}_j + \frac{1}{4} \right) - \frac{1}{2}(1 + \eta r_1) \right\}, \quad (16)$$

$$\hat{f}_{ij}^{(a)} = \frac{1}{4} \left\{ (1 - \eta r_3)(1 + n_{ib}n_{jb}) - r_1(n_{ib} - n_{jb})^2 \right\}, \quad (17)$$

$$\hat{K}_{ij}^{(a)} = \frac{1}{2} \eta (\eta r_1 + r_3)(1 + n_{ib}n_{jb}). \quad (18)$$

The general form of spin-orbital superexchange model (8) suggests that the above symmetry breaking leads indeed to an effective spin model with broken symmetry between magnetic interactions along different cubic axes. By averaging over the orbital operators one finds indeed different effective magnetic exchange interactions, J_c along the c axis and J_{ab} within the ab planes:

$$J_c = \left\langle \hat{f}_{ij}^{(c)} \right\rangle, \quad J_{ab} = \left\langle \hat{f}_{ij}^{(a)} \right\rangle. \quad (19)$$

The interactions in the ab planes could in principle still take two different values in case of finite lattice strain discussed below, making both $\{a, b\}$ axes inequivalent, but here we want just to point out the symmetry breaking between the c axis and the ab planes, which follows from the density distribution (14) and explains the nonequivalence of spin interactions in the C -AF phase of the RVO_3 perovskites [3].

Apart from the superexchange there are in general also interactions due to the couplings to the lattice that control the orbitals. In the cubic vanadates these interactions are expected to be weak, but nevertheless they influence significantly the

spin-orbital fluctuations and decide about the observed properties in the RVO_3 family. We write the orbital interactions, $\propto \tau_i^z \tau_j^z$, induced by the $GdFeO_3$ distortions and by the JT distortions of the lattice using two parameters, V_{ab} and V_c ,

$$\mathcal{H}_V = V_{ab} \sum_{\langle ij \rangle \| c} \tau_i^z \tau_j^z - V_c \sum_{\langle ij \rangle \| c} \tau_i^z \tau_j^z. \quad (20)$$

The orbital interaction along the c axis V_c plays here a crucial role and allows one to switch between the two types of magnetic order, C -AF and G -AF phase [31], stabilizing simultaneously either G -AO or C -AO order.

However, the description in terms of the GKR does not suffice and the ground state of spin-orbital model for the RVO_3 perovskites, which consists of the superexchange and the effective orbital interactions,

$$\mathcal{H}_{S\tau} = \mathcal{H}_J + \mathcal{H}_V. \quad (21)$$

may also be entangled due to the quantum coupling between spin $S = 1$ and orbital $\tau = 1/2$ operators along the c axis, see Eq. (15). In contrast, the orbital fluctuations in the ab planes are quenched due to the occupied c orbitals at each site (14), so spins and orbitals disentangle. Possible entanglement between spin ($\mathbf{S}_i \cdot \mathbf{S}_j$) and orbital ($\tau_i \cdot \tau_j$) operators along the bonds $\langle ij \rangle \| c$ in the RVO_3 perovskites, and the applicability of the GKR to these systems, may be investigated by evaluating intersite spin and orbital correlations (to make these two functions comparable, we renormalized the spin correlations by the factor $\frac{1}{4}$),

$$S_{ij} = \frac{1}{4} \langle \mathbf{S}_i \cdot \mathbf{S}_j \rangle, \quad (22)$$

$$T_{ij} = \langle \tau_i \cdot \tau_j \rangle, \quad (23)$$

and comparing them with each other. A key quantity that measures spin-orbital entanglement is the composite correlation function [10],

$$C_{ij} = \frac{1}{4} \{ \langle \langle \mathbf{S}_i \cdot \mathbf{S}_j \rangle \langle \tau_i \cdot \tau_j \rangle \rangle - \langle \mathbf{S}_i \cdot \mathbf{S}_j \rangle \langle \tau_i \cdot \tau_j \rangle \}. \quad (24)$$

When $C_{ij} = 0$, the spin and orbital operators are disentangled and their MF decoupling is exact, while if $C_{ij} < 0$ — spin and orbital operators are entangled and the MF decoupling not justified.

The numerical results for a 1D chain along the c axis described by vanadate spin-orbital model (21) are shown in Fig. 2. One finds entangled spin-orbital states with all three S_{ij} , T_{ij} and C_{ij} correlations being negative in the spin-singlet ($S = 0$) regime of fluctuating yz and zx orbitals, obtained for $\eta < 0.07$ [Fig. 2(a)]. Therefore, the complementary behavior of spin (22) and orbital (23) correlations is absent in this regime of parameters and the GKR are violated. In addition, composite spin-orbital correlations (24) are here finite ($C_{ij} < 0$), so spin and orbital variables are entangled, and the MF factorization of spin-orbital operators fails. In a similar d^1 model for the perovskite titanates (with $S = 1/2$) one finds even somewhat stronger spin-orbital

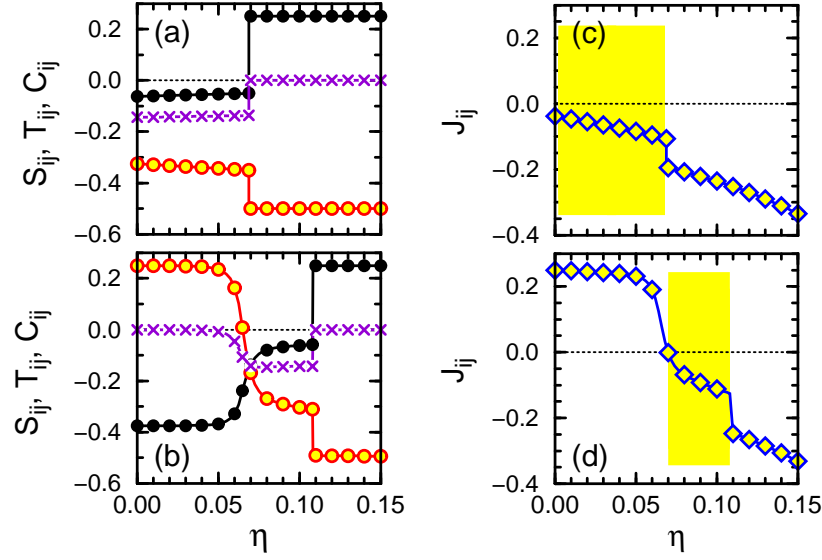


Fig. 2 Evolution of inter-site correlations and exchange constants along the c axis obtained by exact diagonalization of spin-orbital model on a chain of $N = 4$ sites with periodic boundary conditions, with $\hat{J}_{ij}^{(c)}$ and $\hat{K}_{ij}^{(c)}$ given by Eqs. (15) and (16), for increasing Hund's exchange η : (a),(b) inter-site spin S_{ij} (22) (filled circles), orbital (23) (empty circles), and spin-orbital C_{ij} (24) (\times) correlations; (c),(d) the corresponding spin exchange constants J_{ij} (19). In the shaded areas of (c) and (d) the spin correlations $S_{ij} < 0$ do not follow the sign of the exchange constant $J_{ij} < 0$, and the classical GKR are violated. Parameters: (a),(c) $V_c = 0$, and (b),(d) $V_c = J$.

entanglement and the regime of η with $C_{ij} < 0$ is broader (i.e., $\eta < 0.21$) [10]. At the point $\eta = 0$ one recovers then the SU(4) model with $S_{ij} = T_{ij} = C_{ij} = -0.25$, and the ground state is an entangled SU(4) singlet, involving a linear combination of (spin singlet/orbital triplet) and (spin triplet/orbital singlet) states.

To provide further evidence that the GKR do not apply to spin-orbital model (21) in the regime of small η , we compare spin exchange constants J_{ij} (19) shown in Fig. 2(c) with spin correlations S_{ij} (22), see Fig. 2(a). One finds that exchange interaction is formally FM ($J_{ij} < 0$) in the orbital-disordered phase in the regime of $\eta < 0.07$, but it is accompanied by AF spin correlations ($S_{ij} < 0$). Therefore $J_{ij}S_{ij} > 0$ and the ground state energy would be enhanced in an ordered state, when calculated in the MF decoupling of spin-orbital operators [10]. This at first instance somewhat surprising result is a consequence of 'dynamical' nature of exchange constants $\hat{J}_{ij}^{(c)}$ which exhibit large fluctuations [10], measured by the second moment, $\delta J = \{\langle (\hat{J}_{ij}^{(c)})^2 \rangle - J_{ij}^2\}^{1/2}$. For instance, in d^2 model (21) the orbital bond correlations change dynamically from singlet to triplet, resulting in large $\delta J = \frac{1}{4} \{1 - (2T_{ij} + \frac{1}{2})^2\}^{1/2} \simeq 0.247$, i.e., $\delta J > |J_{ij}|$.

Remarkably, finite spin-orbital correlations $C_{ij} < 0$ and similar violation of the GKR are found also at finite orbital interaction (20) induced by the lattice, $V_c > 0$. Representative results obtained for $V_c = J$ are shown in Figs. 2(b) and 2(d). At small η FO order is induced, and in this regime the GKR are followed by the AF/FO phase (similar to the FM/AO phase at large η which also follows the GKR). However, for intermediate Hund's exchange $\eta \sim 0.07$ FO order is destabilized and the entangled AF/AO phase appears, with similar spin, orbital and composite spin-orbital correlations as found before at $V_c = 0$ and $\eta = 0$ [Figs. 2(a)]. Also in this case FM exchange ($J_{ij} < 0$) coexists with AF spin correlations ($S_{ij} < 0$). Thus we conclude that orbital interactions induced by the lattice modify the regime of entangled spin-orbital states in the intermediate AF/AO phase which may be moved to more realistic values of $\eta \sim 0.1$, and cannot eliminate it completely. In addition, the transition between the FO/AF and AO/AF phase is *continuous* [10] due to the structure of orbital superexchange which contains terms (11) responsible for non-conservation of orbital quantum numbers.

3 Experimental evidence of orbital fluctuations in $LaVO_3/YVO_3$

Before discussing the exotic magnetic properties and the phase diagram of the RVO_3 perovskites, we will consider the influence of magnetism on the optical spectra of $LaVO_3$, starting with a general formulation of the theory. While exchange constants may be extracted from the spin-orbital superexchange model (19), it is frequently not realized that virtual charge excitations that contribute to the superexchange are responsible as well for the optical absorption, thus the superexchange and the optical absorption are intimately related to each other via the optical sum rule [33]. This is not so surprising as when electrons are almost localized in a Mott insulator, the only kinetic energy which is left and decides about the optical spectral weight is associated with virtual excitations contributing to superexchange. Therefore, in Mott insulators the thermal evolution of optical spectral weight can be deduced from the superexchange [34]. In a system with orbital degeneracy the optical spectra consist of several multiplet transitions, and the kinetic energy $K_n^{(\gamma)}$ (due to $d-d$ excitations) associated with each of them can be determined from the superexchange (8) using the Hellman-Feynman theorem [32],

$$K_n^{(\gamma)} = 2 \left\langle H_n^{(\gamma)}(ij) \right\rangle. \quad (25)$$

Note that $K_n^{(\gamma)}$ is negative and corresponds to the n 'th multiplet state of the transition metal ion, created by a charge excitation along a bond $\langle ij \rangle \parallel \gamma$. It is obvious that the thermal excitation values $\langle \dots \rangle$ depend sensitively on the magnetic structure, i.e., whether spin correlations on a bond $\langle ij \rangle$ are FM or AF.

Thus it is natural to decompose the optical sum rule which is usually formulated in terms of the *total* kinetic energy for polarization γ ,

$$K^{(\gamma)} = 2J \sum_n \langle H_n^{(\gamma)}(ij) \rangle, \quad (26)$$

into *partial optical sum rules* for individual Hubbard subbands [32],

$$\frac{a_0 \hbar^2}{e^2} \int_0^\infty \sigma_n^{(\gamma)}(\omega) d\omega = -\frac{\pi}{2} K_n^{(\gamma)} = -\pi \langle H_n^{(\gamma)}(ij) \rangle, \quad (27)$$

where $\sigma_n^{(\gamma)}(\omega)$ is the contribution of band n to the optical conductivity for polarization along the γ axis, a_0 is the distance between transition metal ions, and the tight-binding model with nearest neighbor hopping is assumed. Equation (27) provides a practical way of calculating the optical spectral weights from spin-orbital superexchange models, such as the one derived for the RVO_3 perovskites (21). Note that the total optical intensity (26) is of less interest here as it has a much weaker temperature dependence and does not allow one for a direct insight into the nature of the electronic structure. In addition, it might be also more difficult to resolve from experiment.

In order to apply the above theory to the RVO_3 perovskites, we write the superexchange operator $H^{(\gamma)}(ij)$ for a bond $\langle ij \rangle \parallel \gamma$, contributing to operator \mathcal{H}_J (8), as a superposition of $d_i^2 d_j^2 \rightleftharpoons d_i^3 d_j^1$ charge excitations to different upper Hubbard subbands labelled by n [32],

$$H^{(\gamma)}(ij) = \sum_n H_n^{(\gamma)}(ij). \quad (28)$$

One finds the superexchange terms $H_n^{(c)}(ij)$ for a bond $\langle ij \rangle$ along the c axis [32],

$$H_1^{(c)}(ij) = -\frac{1}{3} J r_1 (2 + \mathbf{S}_i \cdot \mathbf{S}_j) \left(\frac{1}{4} - \tau_i \cdot \tau_j \right), \quad (29)$$

$$H_2^{(c)}(ij) = -\frac{1}{12} J (1 - \mathbf{S}_i \cdot \mathbf{S}_j) \left(\frac{7}{4} - \tau_i^z \tau_j^z - \tau_i^x \tau_j^x + 5 \tau_i^y \tau_j^y \right), \quad (30)$$

$$H_3^{(c)}(ij) = -\frac{1}{4} J r_3 (1 - \mathbf{S}_i \cdot \mathbf{S}_j) \left(\frac{1}{4} + \tau_i^z \tau_j^z + \tau_i^x \tau_j^x - \tau_i^y \tau_j^y \right), \quad (31)$$

and $H_n^{(ab)}(ij)$ for a bond in the ab plane,

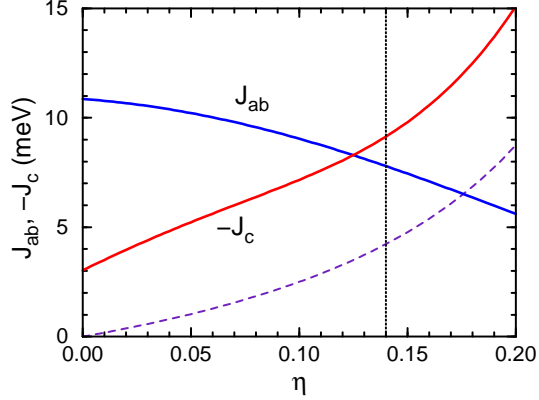
$$H_1^{(ab)}(ij) = -\frac{1}{6} J r_1 (2 + \mathbf{S}_i \cdot \mathbf{S}_j) \left(\frac{1}{4} - \tau_i^z \tau_j^z \right), \quad (32)$$

$$H_2^{(ab)}(ij) = -\frac{1}{8} J (1 - \mathbf{S}_i \cdot \mathbf{S}_j) \left(\frac{19}{12} \mp \frac{1}{2} \tau_i^z \mp \frac{1}{2} \tau_j^z - \frac{1}{3} \tau_i^z \tau_j^z \right), \quad (33)$$

$$H_3^{(ab)}(ij) = -\frac{1}{8} J r_3 (1 - \mathbf{S}_i \cdot \mathbf{S}_j) \left(\frac{5}{4} \mp \frac{1}{2} \tau_i^z \mp \frac{1}{2} \tau_j^z + \tau_i^z \tau_j^z \right). \quad (34)$$

These expressions show that the spin correlations along the c axis and within the ab planes,

Fig. 3 Exchange constants J_{ab} and $-J_c$ (19) calculated from Eqs. (17) and (15) in the C -AF phase of $LaVO_3$ for increasing η (solid lines). Dashed line shows the value of $-J_c$ obtained for classical orbital order (36) according to GKR, $\langle \tau_i \cdot \tau_j \rangle = -\frac{1}{4}$. A representative value of $\eta = 0.14$ (for $U = 5.0$ and $J_H = 0.7$ eV) is marked by dotted line. Parameters of the model (21): $J = 35$ meV, $V_c = V_{ab} = 0$.



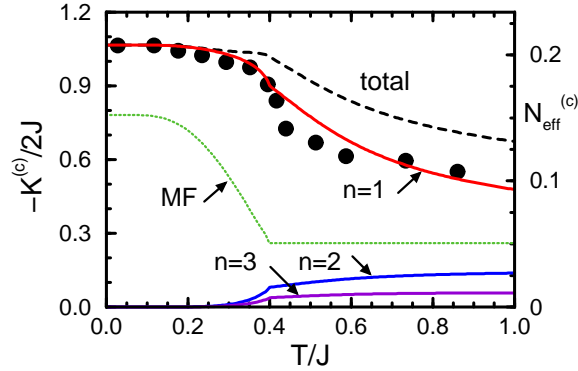
$$s_c = \langle \mathbf{S}_i \cdot \mathbf{S}_j \rangle_c, \quad s_{ab} = \langle \mathbf{S}_i \cdot \mathbf{S}_j \rangle_{ab}, \quad (35)$$

as well as the orbital correlations, play an important role in the intensity distribution in optical spectroscopy. From the form of the above superexchange contributions one sees that high-spin excitations $H_1^{(\gamma)}(ij)$ support the FM coupling while the low-spin ones, $H_2^{(\gamma)}(ij)$ and $H_3^{(\gamma)}(ij)$, contribute with AF couplings.

We have determined the exchange constants in $LaVO_3$ by averaging over the orbital operators, see Eqs. (19). The case of the ab planes is straightforward as only the average densities $\langle n_{ia} \rangle$ and $\langle n_{ib} \rangle$ are needed to determine J_{ab} , and at large η they follow from the G -AO order in these planes. At $\eta = 0$ the orbital correlations along the c axis result from orbital fluctuations in the 1D orbital chain. In this limit the orbital correlations are the same as for the AF Heisenberg chain, i.e., $\langle \tau_i \cdot \tau_j \rangle = -0.4431$ and the ground state is disordered, with $\langle \tau_i^z \rangle = 0$. Nevertheless, for this disordered state the result for J_{ab} is similar as for the G -AO phase [25].

For the disordered (fluctuating) $\{a, b\}$ orbital state at $\eta = 0$, the AF exchange interactions in ab planes (see Fig. 3) result solely from singly occupied c orbitals (14), which are active in these planes and contribute by their double occupancies in excited state with AF superexchange. One expects that the exchange constants along the c axis in the C -AF phase could be deduced from Eqs. (19), as spin and orbital order are complementary [22]. It is quite remarkable that at the same time finite FM interactions $-J_c \simeq 3$ meV are obtained at $\eta = 0$ (Fig. 3). They follow from the orbital fluctuations which dominate at low values of η . This mechanism of FM exchange adds to the one known in systems with real orbital order at finite η — the latter mechanism gradually takes over when η increases and the G -AO order develops and reduces the orbital fluctuations. At finite $\eta > 0$ we used the linear orbital-wave theory [12] to determine the intersite orbital correlations $\langle \tau_i \cdot \tau_j \rangle$ and the order parameter $\langle \tau_i^z \rangle$, for more details see Ref. [25]. At $\eta = 0.14$ representative for $LaVO_3$, the FM interactions are stronger than from AF ones, $|J_c| > J_{ab}$. Indeed, this early prediction of the theory [3] agrees qualitatively with larger average FM

Fig. 4 Kinetic energy $K_n^{(c)}$ (solid lines) for the optical subband n and total $K^{(c)}$ (dashed line) obtained from the spin-orbital model (21). Filled circles show the effective carrier number $N_{eff}^{(c)}$ (in the energy range $\omega < 3$ eV) for LaVO_3 , presented in Fig. 5 of Ref. [35]. Dotted line shows $K_1^{(c)}$ obtained from the MF decoupling (37). Parameters: $\eta = 0.12$, $V_c = 0.9J$, $V_{ab} = 0.2J$.



exchange $J_c < 0$ in the C-AF phase of YVO_3 than the AF exchange $J_{ab} > 0$ in the ab planes, see below.

We emphasize that the strong FM exchange along the c axis follows from the orbital fluctuations, and the rigid G -AO order obtained in the limit of strong orbital interactions $\{V_{ab}, V_c\}$ (20) would give a much weaker FM interaction,

$$J_c^{G\text{-AO}} = -\frac{1}{2}\eta r_1 J, \quad (36)$$

see Fig. 3. The FM interaction $J_c^{G\text{-AO}}$ (36) vanishes at $\eta = 0$, is triggered by finite Hund's exchange η and increases in lowest order linearly with η . This behavior follows the conventional mechanism of FM interactions induced by finite Hund's exchange in the states with AO order, as for instance in KCuF_3 [8] or in LaMnO_3 [2].

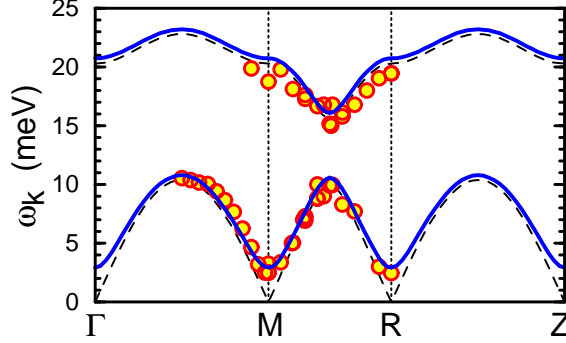
A crucial test of the present theory which demonstrates that orbital fluctuations are indeed present in LaVO_3 , concerns the temperature dependence of the low-energy (high-spin) spectral weight in optical absorption along the c axis $-K_1^{(c)}/2J$. According to experiment [35] it decreases by about 50% between low temperature and $T = 300$ K. In contrast, the result obtained by averaging the high-spin superexchange term $H_1^{(c)}(ij)$ (29) for polarization along the c axis assuming robust G -AO order is,

$$w_{c1}^{G\text{-AO}} = \frac{1}{6}r_1 (s_c + 2), \quad (37)$$

where the spin correlation function s_c (35) is responsible for the entire temperature dependence of the low-energy spectral weight. Equation (37) predicts decrease of w_{c1} of only about 27%, see Fig. 4, and the maximal possible reduction of $K_1^{(c)}$ reached at $s_c = 0$ in the limit of $T \rightarrow \infty$ is by 33%. This result proves that the scenario with frozen G -AO order in LaVO_3 is *excluded by experiment* [5].

In contrast, when a cluster method which allows to include orbital fluctuations along the c axis is used to determine the optical spectral weight from the high-spin superexchange term (29) [32], the temperature dependence resulting from the theory

Fig. 5 Spin-wave dispersions $\omega_{\mathbf{k}}$ obtained in the LSW theory (39) for the C-AF phase of YVO_3 (lines), and measured by neutron scattering at $T = 85$ K [19] (circles). Parameters: $J_{ab} = 2.6$ meV, $J_c = -3.1$ meV, $\delta_s = 0.35$, and $K_z = 0.4$ eV (full lines), $K_z = 0$ (dashed lines). The high symmetry points are: $\Gamma = (0, 0, 0)$, $M = (\pi, \pi, 0)$, $R = (\pi, \pi, \pi)$, $Z = (0, 0, \pi)$.

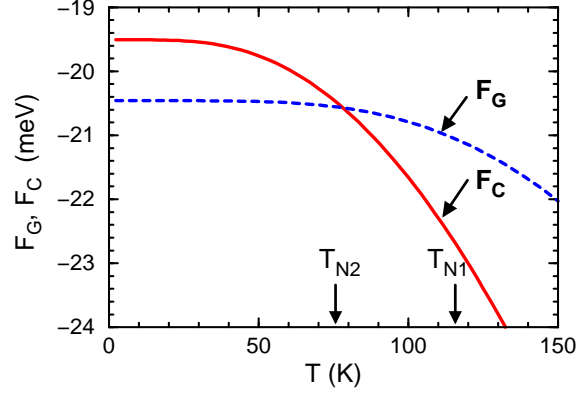


follows the experimental data [35]. This may be considered as a remarkable success of the theory based on the spin-orbital superexchange model derived for the RVO_3 perovskites.

However, the experimental situation in the cubic vanadates is more complex and full of puzzles. One is connected with the second magnetic transition in YVO_3 , as we already mentioned in Sec. 2. The magnetic transition at $T_{N2} = 77$ K is particularly surprising as the staggered moments are approximately parallel to the c axis in the G -AF phase, and rotate above T_{N2} to the ab planes in the C -AF phase, with some small alternating G -AF component along the c axis [36]. While the orientation of spins in C -AF and G -AF phase follow in a straightforward manner from the model, i.e., are consistent with the expected anisotropy due to spin-orbit coupling [31], the observed magnetization reversal with the weak FM component remains puzzling. Therefore, in spite of the suggested mechanism based on the entropy increase in the C -AF phase [25], the lower magnetic transition in YVO_3 remains mysterious. Secondly, the scale of magnetic excitations is considerably reduced for the C -AF phase (by a factor close to two) as compared with the exchange constants deduced from magnons measured in the G -AF phase [19]. In addition, the magnetic order parameter in the C -AF phase of $LaVO_3$ is strongly reduced to $\simeq 1.3\mu_B$, which cannot be explained by the quantum fluctuations in the C -AF phase (being only 6% for $S = 1$ spins [39]). Finally, the C -AF phase of YVO_3 is dimerized. Until now, only this last feature found a satisfactory explanation in the theory [37, 38], see below.

We remark that the observed dimerization in the magnon dispersions may be seen as a signature of *entanglement in excited states* which becomes active at finite temperature. The microscopic reason of the anisotropy in the exchange constants $\mathcal{J}_{c1} \equiv \mathcal{J}_c(1 + \delta_s)$ and $\mathcal{J}_{c2} \equiv \mathcal{J}_c(1 - \delta_s)$ is the tendency of the orbital chain to dimerize, activated by thermal fluctuations in the FM spin chain [38] which support dimerized structure in the orbital sector. As a result one finds alternating stronger $\propto \mathcal{J}_c(1 + \delta_s)$ and weaker $\propto \mathcal{J}_c(1 - \delta_s)$ FM bonds along the c axis in the dimerized C -AF phase (with $\delta_s > 0$). The observed spin waves may be explained by the following effective spin Hamiltonian for this phase (assuming again that the spin and orbital operators may be disentangled which is strictly valid only at $T = 0$):

Fig. 6 Free energies \mathcal{F}_C (C-AF, solid line) and \mathcal{F}_G (G-AF, dashed line) as obtained for the spin-orbital model (21) using the experimental values of magnetic exchange constants in both phases [19]. The experimental magnetic transition temperatures, $T_{N2} \simeq 77$ K and $T_{N1} \simeq 116$ K, are indicated by arrows. Parameters: $J = 40$ meV, $\eta = 0.13$, $V_a = 0.30J$, $V_c = 0.84J$.



$$\mathcal{H}_s = \mathcal{J}_c \sum_{\langle i,i+1 \rangle \| c} [1 + (-1)^i \delta_s] \mathbf{S}_i \cdot \mathbf{S}_{i+1} + \mathcal{J}_{ab}^C \sum_{\langle ij \rangle \| ab} \mathbf{S}_i \cdot \mathbf{S}_j + K_z \sum_i (S_i^z)^2. \quad (38)$$

Following the linear spin-wave theory [25], the magnon dispersion is given by

$$\omega_{\pm}(\mathbf{k}) = 2 \left\{ \left[2 \mathcal{J}_{ab} + |\mathcal{J}_c| + \frac{1}{2} K_z \pm \mathcal{J}_c \eta_{\mathbf{k}}^{1/2} \right]^2 - (2 \mathcal{J}_{ab} \gamma_{\mathbf{k}})^2 \right\}^{1/2}, \quad (39)$$

with

$$\gamma_{\mathbf{k}} = \frac{1}{2} (\cos k_x + \cos k_y), \quad (40)$$

$$\eta_{\mathbf{k}} = \cos^2 k_z + \delta_s^2 \sin^2 k_z. \quad (41)$$

For the numerical evaluation of figure 5 we have used the experimental exchange interactions [19]: $\mathcal{J}_{ab} = 2.6$ meV, $\mathcal{J}_c = -3.1$ meV, $\delta_s = 0.35$. Indeed, large gap is found between two modes halfway in between the M and R points, and between the Z and Γ points (not shown). Two modes measured by neutron scattering [19] (see also figure 1) and obtained from the present theory in the unfolded Brillouin zone are well reproduced by the dimerized FM exchange couplings in spin Hamiltonian (39). We note that a somewhat different Hamiltonian with more involved interactions was introduced in ref. [19], but the essential features seen in the experiment are reproduced already by the present model H_s with a single ion anisotropy term $\propto K_z$.

As the transition between the two magnetic phases, G-AF and C-AF phase, occurs in YVO_3 at finite temperature, the entropy has to play an important role. As mentioned above, the exchange constants found in the C-AF phase of YVO_3 (Fig. 5) are considerably lower than the corresponding values in the G-AF phase, $J_{ab} = J_c \simeq 5.7$ meV [19]. As a result of weaker exchange interactions, the spin entropy of the C phase will grow faster than that of the G phase, and induce the $G \rightarrow C$ transition. However, starting from our model (21) we do not find this strong reduction of energy scale in the C-AF phase. Other mechanism like the fluctuation of n_{xy}

occupancy has been invoked to account for this reduction [25]. Here we will simply adopt the experimental values for the exchange constants in the C -AF phase.

Using linear spin-wave and orbital-wave theory, the spin and orbital entropy normalized per one vanadium ion was calculated and compared for both magnetic phases of YVO_3 [25]. Using the experimental parameters [19] one finds that: (i) the entropy \mathcal{S}_C for the C -AF phase is larger than \mathcal{S}_G for the G -AF phase, and (ii) the spin entropy grows significantly faster with temperature than the orbital entropy for each phase. Therefore, we conclude that the spin entropy gives here a leading contribution and is responsible for a fast decrease of the free energy in the C -AF phase which is responsible for the observed magnetic transition at T_{N2} [25], see Fig. 6.

4 Orbital and magnetic transition in the RVO_3 perovskites

4.1 Spin-orbital-lattice coupling

Experimental studies have shown that the C -AF order is common to the entire family of the RVO_3 vanadates, where $R=Lu, \dots, La$. In general the structural (orbital) transition occurs first. i.e., $T_{N1} < T_{OO}$, except for $LaVO_3$ with $T_{N1} \simeq T_{OO}$ [20, 22]. When the ionic radius r_R decreases, the Néel temperature T_{N1} also decreases, while the orbital transition temperature T_{OO} increases first, passes through a maximum close to YVO_3 , and decreases afterwards when $LuVO_3$ is approached. Knowing that quantum fluctuations and spin-orbital entanglement play so important role in the perovskite vanadates, it is of interest to ask whether the spin-orbital model (21) is able to describe this variation of T_{OO} and T_{N1} with decreasing radius r_R of R ions in RVO_3 [20]. It is clear that the nonmonotonic dependence of T_{OO} on r_R cannot be reproduced just by the superexchange, as a maximum in T_{OO} requires two mechanisms which oppose each other. In fact, the decreasing V–O–V angle (Θ along the c axis) with decreasing ionic radius r_R along the RVO_3 perovskites [40–43] reduces somewhat both the hopping t and superexchange J (6), but we shall ignore this effect here and concentrate ourselves on the leading dependence on orbital correlations which are controlled by lattice distortions.

The model introduced in Ref. [30] to describe the phase diagram of RVO_3 includes the spin-orbital-lattice coupling by the terms: (i) the superexchange H_J (8) between V^{3+} ions in the d^2 configuration with $S = 1$ spins [3], (ii) intersite orbital interactions H_V (20) (which originate from the coupling to the lattice and play an important role in the transition between the C -AF and G -AF phase), (iii) the crystal-field splitting $\propto E_z$ between yz and zx orbitals, and (iv) orbital-lattice term $\propto gu$ which induces orbital polarization when the lattice strain (distortion) u increases. The Hamiltonian consists thus of several terms [30],

$$\mathcal{H} = \mathcal{H}_J + \mathcal{H}_V(\vartheta) + E_z(\vartheta) \sum_i e^{i\mathbf{R}_i \cdot \mathbf{Q}} \tau_i^z - gu \sum_i \tau_i^x + \frac{1}{2} NK \{u - u_0(\vartheta)\}^2. \quad (42)$$

Except for the superexchange \mathcal{H}_J (8), all the other terms in Eq. (42) depend on the tilting angle ϑ , which we use to parameterize the RVO_3 perovskites below. It is related to the V–O–V angle $\Theta = \pi - 2\vartheta$, which decreases with increasing ionic radius r_R ($\Theta = 180^\circ$ corresponds to an ideal perovskite structure). By analyzing the structural data of the RVO_3 perovskites [40–43] one arrives at the following empirical relation between r_R and ϑ :

$$r_R = r_0 - \alpha \sin^2 2\vartheta, \quad (43)$$

with $r_0 = 1.5 \text{ \AA}$ and $\alpha = 0.95 \text{ \AA}$.

The crystal-field splitting of $\{yz, zx\}$ orbitals ($E_z > 0$) alternates in the ab planes and is uniform along the c axis, with a modulation vector $\mathbf{Q} = (\pi, \pi, 0)$ in cubic notation — it supports the C -AO order, and not the observed (weak) C -AO order. The orbital interactions induced by the distortions of the VO_6 octahedra and by $GdFeO_3$ distortions of the lattice, $V_{ab} > 0$ and $V_c > 0$, also favor the C -AO order (like $E_z > 0$). The orbital interaction V_c counteracts the orbital superexchange $\propto J$ (16), and has only rather weak dependence on ϑ , so it suffices to choose a constant $V_c = 0.26J$ to reproduce an almost simultaneous onset of spin and orbital order in $LaVO_3$, with $T_{OO} \simeq T_{N1}$, as observed [20]. One finds $T_{N1}^{\text{exp}} = 147 \text{ K}$ taking $J = 200 \text{ K}$ in the present model (42), which reproduces well the experimental value $T_{N1}^{\text{exp}} = 143 \text{ K}$ for $LaVO_3$ [20].

The last two terms in Eq. (42) describe the orbital-lattice coupling via the orthorhombic strain $u = (b - a)/a$, where a and b are the lattice parameters of the $Pbnm$ structure, K is the force constant, and N is the number of V^{3+} ions. Unlike E_z , the coupling $gu > 0$ acts as a transverse field in the pseudospin space and favors that one of the two linear combinations $\frac{1}{\sqrt{2}}(|a\rangle_i \pm |b\rangle_i)$ of active t_{2g} orbitals is occupied at site i . By minimizing the energy over u , one finds

$$g_{\text{eff}}(\vartheta; T) \equiv gu(\vartheta; T) = gu_0(\vartheta) + \frac{g^2}{K} \langle \tau^x \rangle_T, \quad (44)$$

which shows that the global distortion $u(\vartheta; T)$ consists of (i) a pure lattice contribution $u_0(\vartheta)$, and (ii) a contribution due the orbital polarization $\propto \langle \tau^x \rangle$ which is determined self-consistently.

4.2 Dependence on lattice distortion

In order to investigate the phase diagram of the RVO_3 perovskites one needs still information on the functional dependence of the parameters $\{E_z, V_{ab}, g_{\text{eff}}\}$ of the microscopic model (42) on the tilting angle ϑ . The $GdFeO_3$ -like distortion is parametrized by two angles $\{\vartheta, \varphi\}$ describing rotations around the b and c cubic axes, as explained in Ref. [44]. Here we adopted a representative value of $\varphi = \vartheta/2$, similar as in the perovskite titanates. Therefore, we used only a single rotation angle ϑ in Eq. (42), which is related to the ionic size by Eq. (43). Functional dependence

of the crystal-field splitting $E_z \propto \sin^3 \vartheta \cos \vartheta$ on the angle ϑ may be derived from the point charge model [30], using the structural data for the RVO_3 perovskites [40–43]. It is expected that the functional dependence of V_{ab} follows the crystal-field term, so we write:

$$E_z(\vartheta) = J v_z \sin^3 \vartheta \cos \vartheta, \quad (45)$$

$$V_{ab}(\vartheta) = J v_{ab} \sin^3 \vartheta \cos \vartheta. \quad (46)$$

Qualitatively, increasing E_z and V_{ab} with increasing lattice distortion and tilting angle ϑ do favor the orbital order, so the temperature T_{OO} is expected to increase.

A maximum observed in the dependence of T_{OO} on r_R (or ϑ) may be reproduced within the present model (42) only when a competing orbital polarization interaction $g_{\text{eff}}(\vartheta; T)$ (44) increases faster with ϑ when the ionic radius r_R is reduced than $\{E_z, V_{ab}\}$. Both u_0 and $\langle \tau^x \rangle$ in Eq. (44) are expected to increase with increasing tilting angle ϑ . Below we present the results obtained with a semiempirical relation,

$$g_{\text{eff}}(\vartheta) = J v_g \sin^5 \vartheta \cos \vartheta, \quad (47)$$

as postulated in Ref. [30]. Altogether, model (21) depends on three parameters: $\{v_z, v_{ab}, v_g\}$ which could be selected [30] to reproduce the observed dependence of orbital and magnetic transition temperature on the ionic radius r_R in the RVO_3 perovskites, see below.

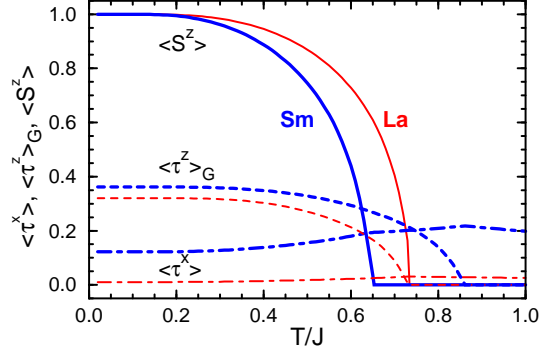
4.3 Evolution of spin and orbital order in RVO_3

Hamiltonian (42) poses a many-body problem which includes an interplay between spin, orbital, and lattice degrees of freedom. A standard approach to investigate the onset of spin and orbital order is to use the mean-field (MF) theory with on-site order parameters $\langle S^z \rangle$ (corresponding to C-AF phase) and

$$\langle \tau^z \rangle_G \equiv \frac{1}{2} \left| \langle \tau_i^z - \tau_j^z \rangle \right|, \quad (48)$$

as well as the coupling between them which modifies the MF equations, similar to the situation encountered in the Ashkin-Teller model [45]. This approach was successfully implemented to determine the orbital and magnetic transition temperature, T_{OO} and T_{N1} in LaMnO_3 [2]. It was also applied to the RVO_3 perovskites [46] to demonstrate that either spin or orbital order may occur first at decreasing temperature, depending on the amplitude of hopping parameters. However, Such a MF approach uses only on-site order parameters and cannot suffice when orbital fluctuations also contribute, e.g. stabilizing the C-AF phase in LaVO_3 [3] — then it becomes essential to determine self-consistently the above on-site order parameters together with orbital singlet correlations (23) on the bonds $\langle ij \rangle \parallel c$. The simplest approach which allows us to determine these correlations is a cluster MF theory for a

Fig. 7 The orbital polarization $\langle \tau^x \rangle$ (dashed-dotted lines), G -type orbital order parameter $\langle \tau^z \rangle_G$ (48) (dashed lines), and spin order parameter $\langle S^z \rangle$ (solid lines) for LaVO_3 and SmVO_3 (thin and heavy lines). Parameters: $V_c = 0.26J$, $v_z = 17$, $v_{ab} = 22$, $v_g = 740$.



bond coupled to effective spin and orbital symmetry breaking fields which originate from its neighbors in an ordered phase. The respective transition temperatures are obtained when $\langle S^z \rangle > 0$ ($\langle S^z \rangle = 0$) for $T < T_{N1}$ ($T > T_{N1}$), and $\langle \tau^z \rangle_G > 0$ ($\langle \tau^z \rangle_G = 0$) for $T < T_{OO}$ ($T > T_{OO}$).

Making a proper selection of the model parameters $\{v_z, v_{ab}, v_g\}$ one is able to reproduce the experimental phase diagram for the onset of G -AO and C -AF order in the $R\text{VO}_3$ family in the entire range of r_R , see below. We start with presenting an example of the orbital and spin phase transition in LaVO_3 and in SmVO_3 , see Fig. 7. By selecting $V_c = 0.26J$ both G -AO and C -AF order occur simultaneously in LaVO_3 below $T_{OO} = T_{N1} \simeq 0.73J$. The crystal field splitting E_z , orbital interaction V_{ab} , and the coupling to the lattice g_{eff} are rather small and do not influence the order in LaVO_3 . We emphasize that orbital correlations along the c axis are here practically as in the AF Heisenberg chain, $\langle \tau_i \cdot \tau_j \rangle \simeq -0.44$, and the orbital order is considerably reduced, $\langle \tau^z \rangle_G \simeq 0.32$. The orbital polarization in LaVO_3 $\langle \tau^x \rangle \simeq 0.03$ is rather weak at T_{N1} , and is further reduced with decreasing $T < T_{OO}$. Note that also spin order parameter is expected to be reduced below $\langle S^z \rangle = 1$, but weak quantum fluctuations in the C -AF phase [39] were neglected here. In contrast, in SmVO_3 the phase transitions separate: the orbital transition occurs first at $T_{OO} \simeq 0.86J$, and the magnetic one follows at a lower $T_{N1} \simeq 0.65J$. Already in this case the transverse orbital polarization is considerably increased, with $\langle \tau^x \rangle \simeq 0.20$ at T_{N1} (see Fig. 7), and further increases with decreasing r_R (not shown). Note that the polarization $\langle \tau^x \rangle$ does not change close to T_{OO} , and only below T_{N1} gets weakly reduced due to the developing magnetic order, in agreement with experiment [43]. The G -OO parameter is here stronger as the singlet orbital fluctuations are not so pronounced when $T \rightarrow 0$, being $\langle \tau^z \rangle_G \simeq 0.37$.

The key features of the present spin-orbital system which drive the observed dependence of T_{OO} and T_{N1} on r_R [20] is the evolution of intersite orbital correlations are: (i) the gradual increase of the orbital interactions $K_{ab} \tau_i^z \tau_j^z$ [Fig. 8(a)], and (ii) the reduction of orbital fluctuations on the bonds along the c axis, described by the bond singlet correlations $\langle \tau_i \cdot \tau_j \rangle$ [Fig. 8(b)]. The parameter K_{ab} in Fig. 8(a) consists of the superexchange contribution $\propto J$ (18) and orbital interaction V_{ab} (20) induced by the lattice distortion. While the superexchange does not change with decreasing

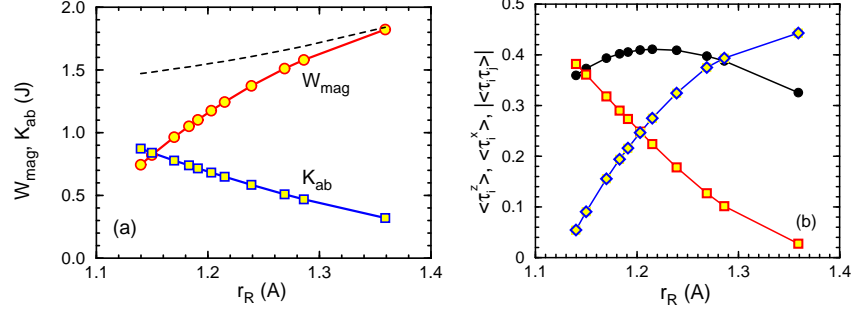


Fig. 8 (a) The width of magnon band W_{C-AF} for finite g_{eff} (circles) and without orbital-strain coupling ($g_{\text{eff}} = 0$, dashed), and orbital interactions in ab planes K_{ab} (squares) in the C -AF phase of cubic vanadates (the points correspond to the RVO_3 compounds of Fig. 9). (b) Evolution of the orbital order parameter $\langle \tau_i^z \rangle_G$ (filled circles), transverse orbital polarization $\langle \tau_i^x \rangle$ (squares), and orbital intersite correlations $|\langle \tau_i \cdot \tau_j \rangle|$ (diamonds) along c axis at $T = 0$. Parameters: $v_z = 17$, $v_{ab} = 22$, $v_g = 740$.

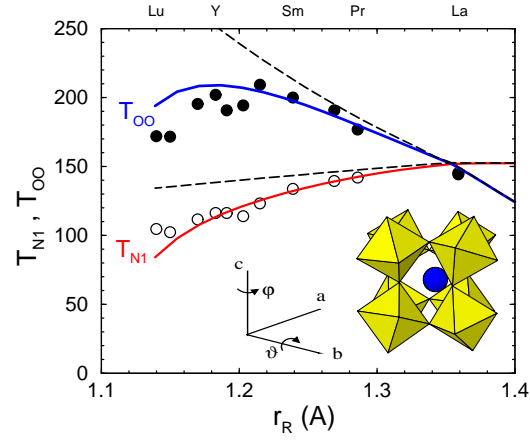
r_R , the latter term increases and induces the increase of T_{OO} from LaVO_3 to YVO_3 . This increase is similar to that observed in the RMnO_3 manganites [21]. Thereby the bond angle Θ decreases from 157.4° in LaVO_3 to 144.8° in YVO_3 .

While the singlet correlations are drastically suppressed from LaVO_3 towards LuVO_3 , the orbital order parameter $\langle \tau^z \rangle_G$ somewhat increases from LaVO_3 to SmVO_3 (see also Fig. 7). At the same time the orbital polarization $\langle \tau^x \rangle$ increases and soon becomes as important as the orbital order parameter, i.e., $\langle \tau^x \rangle \simeq \langle \tau^z \rangle_G$. Further increase of the orbital polarization towards LuVO_3 suppresses the G -AO parameter, so $\langle \tau^z \rangle_G$ passes through a maximum and decreases for $r_R < 1.22$ Å.

It is remarkable that the above changes in orbital correlations induced by the lattice suppress gradually the magnetic interactions in the C -AF phase, although the value of J remains unchanged. This is well visible in the total width of the magnon band, $W_{C-AF} = 4(J_{ab} + |J_c|)$ (at $T = 0$) [25], shown in Fig. 8(a), being reduced from $\sim 1.84J$ in LaVO_3 to $\sim 1.05J$ in YVO_3 . This large reduction qualitatively agrees with the rather small values of the exchange constants in the C -AF phase of YVO_3 [19], see also Fig. 5. This reduction is caused by the suppression of the singlet orbital correlations $\langle \tau_i \cdot \tau_j \rangle$ by the increasing coupling to the lattice $g_{\text{eff}}(\vartheta)$ when r_R decreases. Note also that this effect would be rather small for $g_{\text{eff}} = 0$ — this behavior is excluded by experiment.

Following Ref. [30], we argue that the gradual reduction of the orbital singlet correlations in favor of increasing orbital polarization is responsible for the evolution of the orbital transition temperature T_{OO} in the experimental phase diagram of Fig. 9, which is reproduced by the theory in the entire range of available r_R . The transition temperature T_{OO} changes in a nonmonotonic way, similar to the orbital order parameter $\langle \tau^z \rangle_G$ at $T = 0$ [Fig. 8(b)]. After analyzing the changes in the orbital correlations, we see that the physical reasons of the decrease of T_{OO} for small (large) r_R are quite different. While the orbital fluctuations dominate and largely

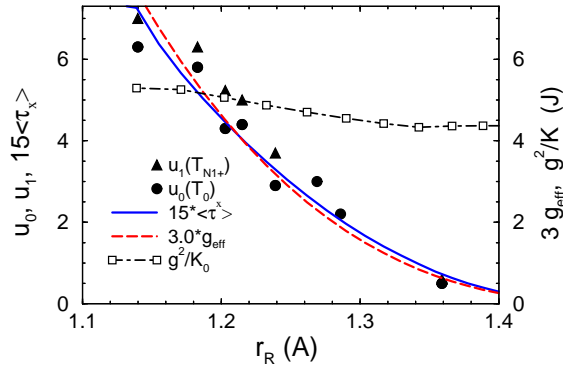
Fig. 9 The orbital T_{OO} and magnetic T_{N1} transition temperature for varying r_R in the RVO_3 perovskites, obtained from model (42) for: $v_g = 740$ (solid lines) and $v_g = 0$ (dashed lines). Circles show the experimental data of Ref. [20]. The inset shows the $GdFeO_3$ -type distortion, with the rotation angles ϑ and φ . Other parameters as in Fig. 8. This figure is reproduced from Ref. [30].



suppress the orbital order in $LaVO_3$, the orbital polarization takes over near YVO_3 and competes with G -AO order.

While the above fast dependence on the tilting angle ϑ of VO_6 octahedra in the RVO_3 family was introduced in order to reproduce the experimentally observed dependence of T_{OO} on r_R , see Fig. 9, it may be justified *a posteriori*. It turns out that the dependence of g_{eff} on the ionic radius r_R in Eq. (47) follows the actual lattice distortion u in RVO_3 measured at $T = 0$ (u_0), or just above T_{N1} (u_1) [30]. Also the orbital polarization $\langle \tau^x \rangle$ is approximately $\propto \sin^5 \vartheta \cos \vartheta$, and follows the same fast dependence of g_{eff} (ϑ for the RVO_3 perovskites (Fig. 10). This result is somewhat unexpected, as information about the actual lattice distortions has not been used in constructing the microscopic model (21). These results indicate that the bare coupling parameters $\{g, K\}$ are nearly constant and independent of r_R , which may be treated as a prediction of the theory to be verified by future experiments.

Fig. 10 Experimental distortion (in percent) at $T = 0$ (u_0 , circles) and above T_{N1} (u_1 , triangles) for the RVO_3 compounds [40, 41, 43], compared with the orbital polarization $\langle \tau^x \rangle_{T=0}$ and with g_{eff} (47); g_{eff} and g^2/K are in units of J . Squares show the upper bound for g^2/K predicted by the theory. Parameters: $v_z = 17$, $v_{ab} = 22$, $v_g = 740$. This figure is reproduced from Ref. [30].



5 Summary and outlook

Summarizing, spin-orbital superexchange model (42) augmented by orbital-lattice couplings provides an explanation of the experimental variation of the orbital T_{OO} and magnetic T_{N1} transition temperatures for the whole class of the RVO_3 perovskites. A more complete theoretical understanding including a description of the second magnetic transition from C -AF to G -AF phase, which occurs at T_{N2} for small ionic radii r_R [47], remains to be addressed by future theory, which should include the spin-orbit relativistic coupling [31].

We conclude by mentioning a few open issues and future directions of research in the field of perovskite vanadates. Rapid progress of the field of orbital physics results mainly from experiment, and is triggered by the synthesis of novel materials. Although experiment is ahead of theory in most cases, there are some exceptions. One of them was a theoretical prediction of the energy and dispersion of orbital excitations [12, 48, 49]. Only recently orbital excitations (orbitons) could be observed by Raman scattering in the Mott insulators $LaTiO_3$ and $YTiO_3$ [50, 51]. They were also identified in the optical absorption spectra of YVO_3 and $HoVO_3$ [52]. The exchange of two orbitals along the c axis in the intermediate C -AF phase was shown to contribute to the optical conductivity $\sigma(\omega)$.

An interesting question which arises in this context is the carrier propagation in a Mott insulator with orbital order. This problem is rather complex as in a spin-orbital polaron, created by doping of a single hole, both spin and orbital excitations contribute to the hole scattering [24], which may even become localized by string excitations as in the t - J^z model [53]. Indeed, the coupling to orbitons increases the effective mass of a moving hole in e_g systems [54]. The orbital part of the superexchange is classical (compass-like) in t_{2g} systems, but nevertheless the hole is not confined as weak quasiparticle dispersion arises from three-site processes [55, 56].

As in the doped manganites, also in doped $R_{1-x}(Sr,Ca)_xVO_3$ systems the G -AO order gradually disappears [57]. The C -AF spin order survives, however, in a broad range of doping, in contrast to $La_{1-x}Sr_xMnO_3$, where FM order replaces the A -AF phase already at $x \sim 0.10$, and is accompanied by the e_g orbital liquid [58] at higher doping. It is quite remarkable that the complementary G -AF/ C -AO order is fragile and disappears in $Y_{1-x}Ca_xVO_3$ already at $x = 0.02$ [57]. The doped holes in C -AF/ G -AO phase are localized in polaron-like states [59], so the pure electronic model such as the one of Ref. [55] is too crude to capture both the evolution of the spin-orbital order in doped vanadates and the gradual decrease of the energy scale for spin-orbital fluctuations. Theoretical studies at finite hole concentration are still nonexistent in 3D models, but one may expect a transition from a phase with AF order to a phase with FM spin polarization at large Hund's coupling, as shown both for e_g [13] and t_{2g} [57] systems.

A few representative problems related to the properties of RVO_3 perovskites discussed above demonstrate that the orbital physics is a very rich field, with in-

trinsically frustrated interactions and rather exotic ordered or disordered phases, with their behavior dominated by quantum fluctuations. While valuable information about the electronic structure is obtained from density functional theory [61], the many-body aspects have to be studied simultaneously using models of correlated electrons. The RVO_3 perovskites remain an interesting field of research, as it turned out that electron-lattice coupling is here not strong enough to suppress (quench) the orbital fluctuations [30]. Thus the composite quantum fluctuations described by the spin-orbital model (42) remain active. Nevertheless, there is significant control of the electronic properties due to the electron-lattice coupling. Thus, the lattice distortions may also influence the onset of magnetic order in systems with active orbital degrees of freedom. If they are absent and the lattice is frustrated in addition, a very interesting situation arises, with strong tendency towards truly exotic quantum states [15]. Examples of this behavior were considered recently for the triangular lattice, both for e_g orbitals in $LiNiO_2$ [62] and t_{2g} orbitals in $NaTiO_2$ [63]. None of these models could really be solved, but generic tendency towards dimer correlations with spin singlets on the bonds for particular orbital states has been shown. Yet, the question whether novel types of orbital order, such as e.g. nematic order in spin models [64], could be found in certain situations remains open.

Acknowledgements It is our great pleasure to thank G. Khaliullin and L.F. Feiner for very stimulating collaboration which significantly contributed to our present understanding of the subject. We thank B. Keimer, G.A. Sawatzky, Y. Tokura and particularly C. Ulrich for numerous insightful discussions. A.M. Oleś acknowledges financial support by the Foundation for Polish Science (FNP) and by the Polish Ministry of Science and Education under Project No. N202 068 32/1481.

References

1. Y. Tokura, N. Nagaosa, *Science* **288**, 462 (2000)
2. L.F. Feiner, A.M. Oleś, *Phys. Rev. B* **59**, 3295 (1999)
3. G. Khaliullin, P. Horsch, A.M. Oleś, *Phys. Rev. Lett.* **86**, 3879 (2001)
4. A.M. Oleś, P. Horsch, G. Khaliullin, L.F. Feiner, *Phys. Rev. B* **72**, 214431 (2005)
5. S. Miyasaka, S. Onoda, Y. Okimoto, J. Fujioka, M. Iwama, N. Nagaosa, Y. Tokura, *Phys. Rev. Lett.* **94**, 076405 (2005)
6. J.-Q. Yan, J.-S. Zhou, J.B. Goodenough, Y. Ren, J.G. Cheng, S. Chang, J. Zarestky, O. Garlea, A. Liobet, H.D. Zhou, Y. Sui, W.H. Su, R.J. McQueeney, *Phys. Rev. Lett.* **99**, 197201 (2007)
7. K.I. Kugel, D.I. Khomskii, *Sov. Phys. Usp.* **25**, 231 (1982)
8. L.F. Feiner, A.M. Oleś, J. Zaanen, *Phys. Rev. Lett.* **78**, 2799 (1997)
9. J. van den Brink, *New J. Phys.* **6**, 201 (2004)
10. A.M. Oleś, P. Horsch, L.F. Feiner, G. Khaliullin, *Phys. Rev. Lett.* **96**, 147205 (2006)
11. B. Frishmuth, F. Mila, M. Troyer, *Phys. Rev. Lett.* **82**, 835 (1999)
12. J. van der Brink, P. Horsch, F. Mack, A.M. Oleś, *Phys. Rev. B* **59**, 6795 (1999)
13. M. Daghofer, A.M. Oleś, W. von der Linden, *Phys. Rev. B* **70**, 184430 (2004)
14. L.F. Feiner, A.M. Oleś, *Phys. Rev. B* **71**, 144422 (2005)
15. G. Khaliullin, *Prog. Theor. Phys. Suppl.* **160**, 155 (2005)
16. D.I. Khomskii, M.V. Mostovoy, *J. Phys. A* **36**, 9197 (2003)
17. J. Dorier, F. Becca, F. Mila, *Phys. Rev. B* **72**, 024448 (2005)
18. W. Brzezicki, J. Dziarmaga, A.M. Oleś, *Phys. Rev. B* **75** 134415 (2007)

19. C. Ulrich, G. Khaliullin, J. Sirker, M. Reehuis, M. Ohl, S. Miyasaka, Y. Tokura, B. Keimer, Phys. Rev. Lett. **91**, 257202 (2003)
20. S. Miyasaka, Y. Okimoto, M. Iwama, Y. Tokura, Phys. Rev. B **68**, 100406 (2003)
21. J.-S. Zhou, J.B. Goodenough, Phys. Rev. Lett. **96**, 247202 (2006)
22. S. Miyasaka, J. Fujioka, M. Iwama, Y. Okimoto, Y. Tokura, Phys. Rev. B **73**, 224436 (2006)
23. L.F. Feiner, A.M. Oleś, J. Zaanen, J. Phys.: Condens. Matter **10**, L555 (1998)
24. J. Zaanen, A.M. Oleś, Phys. Rev. B **48**, 7197 (1993)
25. A.M. Oleś, P. Horsch, G. Khaliullin, Phys. Rev. B **75**, 184434 (2007)
26. J.S. Griffith, *The Theory of Transition Metal Ions* (Cambridge University Press, Cambridge, 1971)
27. A. Weiße, H. Fehske, New J. Phys. **6** 158 (2004)
28. A.M. Oleś, L.F. Feiner, J. Zaanen, Phys. Rev. B **61**, 6257 (2000)
29. M. De Raychaudhury, E. Pavarini, O.K. Andersen, Phys. Rev. Lett. **99**, 126402 (2007)
30. P. Horsch, A.M. Oleś, L.F. Feiner, G. Khaliullin, Phys. Rev. Lett. **100**, 167205 (2008)
31. P. Horsch, G. Khaliullin, A.M. Oleś, Phys. Rev. Lett. **91**, 257203 (2003)
32. G. Khaliullin, P. Horsch, A.M. Oleś, Phys. Rev. B **70**, 195103 (2004)
33. D. Baeriswyl, J. Carmelo, A. Luther, Phys. Rev. B **33**, 7247 (1986)
34. M. Aichhorn, P. Horsch, W. von der Linden, M. Cuoco, Phys. Rev. B **65**, 201102 (2002)
35. S. Miyasaka, Y. Okimoto, Y. Tokura, J. Phys. Soc. Jpn. **71**, 2086 (2002)
36. Y. Ren, T.T.M. Palstra, D.I. Khomskii, A.A. Nugroho, A.A. Menovsky, G.A. Sawatzky, Phys. Rev. B **62**, 6577 (2000)
37. J. Sirker, G. Khaliullin, Phys. Rev. B **67**, 100408(R) (2003)
38. J. Sirker, A. Herzog, A.M. Oleś, P. Horsch, Phys. Rev. Lett. **101**, 157204 (2008)
39. M. Raczkowski, A.M. Oleś, Phys. Rev. B **66**, 094431 (2002)
40. Y. Ren, A.A. Nugroho, A.A. Menovsky, J. Stempfer, U. Rütt, F. Iga, T. Takabatake, C.W. Kimball, Phys. Rev. B **67**, 014107 (2003)
41. M. Reehuis, C. Ulrich, P. Pattison, B. Ouladdiaf, M.C. Rheinstädter, M. Ohl, L.P. Regnault, M. Miyasaka, Y. Tokura, B. Keimer, Phys. Rev. B **73**, 094440 (2006)
42. M.H. Sage, G.R. Blake, G.J. Nieuwenhuys, T.T.M. Palstra, Phys. Rev. Lett. **96**, 036401 (2006)
43. M.H. Sage, G.R. Blake, C. Marquina, T.T.M. Palstra, Phys. Rev. B **76**, 195102 (2007)
44. E. Pavarini, A. Yamasaki, J. Nuss, O.K. Andersen, New J. Phys. **7**, 188 (2005)
45. R.V. Ditzian, J.R. Banavar, G.S. Grest, L.P. Kadanoff, Phys. Rev. B **22**, 2542 (1980)
46. T.N. De Silva, A. Joshi, M. Ma, F.C. Zhang, Phys. Rev. B **68**, 184402 (2003)
47. D.A. Mazurenko, A.A. Nugroho, T.T.M. Palstra, P.H.M. van Loosdrecht, Phys. Rev. Lett. **101**, 245702 (2008)
48. S. Ishihara, J. Inoue, S. Maekawa, Phys. Rev. B **55**, 8280 (1997)
49. J. van den Brink, Phys. Rev. Lett. **87**, 217202 (2001)
50. C. Ulrich, A. Gössling, M. Grüninger, M. Guennou, H. Roth, M. Cwik, T. Lorenz, G. Khaliullin, B. Keimer, Phys. Rev. Lett. **97**, 157401 (2006)
51. C. Ulrich, G. Ghiringhelli, A. Piazzalunga, L. Braicovich, N.B. Brookes, H. Roth, T. Lorenz, B. Keimer, Phys. Rev. B **77**, 113102 (2008)
52. E. Benckiser, R. Rückamp, T. Möller, T. Taetz, A. Möller, A.A. Nugroho, T.T.M. Palstra, G.S. Uhrig, M. Grüninger, New J. Phys. **10**, 053027 (2008)
53. G. Martínez, P. Horsch, Phys. Rev. B **44**, 317 (1991)
54. J. van den Brink, P. Horsch, A.M. Oleś, Phys. Rev. Lett. **85**, 5174 (2000)
55. M. Daghofer, K. Wohlfeld, A.M. Oleś, E. Arrigoni, P. Horsch, Phys. Rev. Lett. **100**, 066403 (2008)
56. K. Wohlfeld, M. Daghofer, A.M. Oleś, P. Horsch, Phys. Rev. B **78**, 214423 (2008)
57. J. Fujioka, S. Miyasaka, Y. Tokura, Phys. Rev. B **72**, 024460 (2005)
58. A.M. Oleś, L.F. Feiner, Phys. Rev. B **65**, 052414 (2000)
59. J. Fujioka, S. Miyasaka, Y. Tokura, Phys. Rev. B **77**, 144402 (2008)
60. J. Sirker, J. Damerau, A. Klümper, Phys. Rev. B **78**, 235125 (2008)
61. I.V. Solovyev, J. Phys.: Condens. Matter **20**, 293201 (2008).
62. A.J.W. Reitsma, L.F. Feiner, A.M. Oleś, New J. Phys. **7**, 121 (2005)
63. B. Normand, A.M. Oleś, Phys. Rev. B **78**, 094427 (2008)
64. N. Shannon, T. Momoi, P. Sindzingre, Phys. Rev. Lett. **96**, 027213 (2006)